A Logarithmic Quantization Index Modulation for Perceptually Better Data Hiding

Nima Khademi Kalantari, *Student Member, IEEE*, and Seyed Mohammad Ahadi, *Senior Member, IEEE*

***Abstract*—In this paper, a novel arrangement for quantizer levels in the Quantization Index Modulation (QIM) method is proposed. Due to perceptual advantages of logarithmic quantization, and in order to solve the problems of a previous logarithmic quantization-based method, we used the compression function of μ-Law standard for quantization. In this regard, the host signal is first transformed into the logarithmic domain using the μ-Law compression function. Then, the transformed data is quantized uniformly and the result is transformed back to the original domain using the inverse function. The scalar method is then extended to vector quantization. For this, the magnitude of each host vector is quantized on the surface of hyperspheres which follow logarithmic radii. Optimum parameter μ for both scalar and vector cases is calculated according to the host signal distribution. Moreover, inclusion of a secret key in the proposed method, similar to the dither modulation in QIM, is introduced. Performance of the proposed method in both cases is analyzed and the analytical derivations are verified through extensive simulations on artificial signals. The method is also simulated on real images and its performance is compared with previous scalar and vector quantization-based methods. Results show that this method features stronger a watermark in comparison with conventional QIM and, as a result, has better performance while it does not suffer from the drawbacks of a previously proposed logarithmic quantization algorithm.**

***Index Terms*—Digital watermarking, generalized Gaussian distribution, logarithmic quantization, Quantization Index Modulation (QIM).**

I. Introduction

DIGITAL watermarking has been widely studied during recent years for the purposes of copyright protection, authentication, fingerprinting, copy protection, etc. Generally, watermarking is the technology of embedding a useful data (watermark data) within a host signal. This embedding should not substantially degrade the perceptual quality of the host signal.

Among many watermarking schemes presented so far, the class of Quantization Index Modulation (QIM) methods proposed in [1] has grabbed the attention of researchers due to its good rate distortion-robustness tradeoffs. According to QIM, the watermark data is embedded by quantizing the host signal features using a set of quantizers, each of which associated with a different message. QIM is a blind method in which the original signal is not needed to extract the watermark data. Also, the embedding and extraction functions are simple and easy to implement.

The main problem of QIM is designing codebooks of the quantizers. Many previously proposed quantization-based data hiding methods used uniform quantization [2]–[4]. The uniform quantization is optimum when the host signal is uniformly distributed. For the hosts with nonuniform distributions, there exists a set of optimum quantizer levels, by use of which, quantization introduces minimum distortion to the host signal. Furthermore, uniform quantization results in host-independent watermark signal. This way, the watermark signal can be easily estimated by averaging on a set of watermarked signals. Also, by uniform quantization, the perceptual characteristics of the host signal are not considered and the watermark power is distributed uniformly within the host signal, which introduces perceptible distortions in some parts of it.

A quantization-based watermarking approach in the logarithmic domain has been proposed in [5] which features perceptual advantages. There, a simple logarithm function, i.e., $f(x) = \ln(|x|)$, has been used for quantization. In this regard, first, the host signal features are transformed using the logarithm function. Then, quantization is performed using uniform step sizes on transformed signal in order to embed data within host signal. The watermarked signal is obtained using the inverse of logarithm function. Uniform and logarithmic quantization-based methods can be compared with additive [6] and multiplicative [7] spread spectrum methods. According to [8], multiplicative methods are preferred to additive ones since a disturbance proportional to the signal strength is more difficult to perceive. Thus, multiplicative schemes lead to stronger watermark embedding while keeping the quality of watermarked audio at an acceptable level. Furthermore, multiplicative methods are more secure than additive ones since, in the former, a host signal dependent watermark is obtained and it is more difficult to estim]ate the watermark by averaging on a set of watermarked signals [8]. This attack is called collusion attack [9], [10] in the watermarking literature and is applicable when copies of multiple works with the same watermark embedded within are available.

Similar advantages could be counted for logarithmic quantization in comparison with uniform quantization. As an example, in images, when quantization is performed on AC coefficients, since eye is less sensitive to the complex part of image and this area has stronger AC component, quantization with larger step

Manuscript received March 07, 2009; revised December 23, 2009. First published March 15, 2010; current version published May 14, 2010. Parts of this work were presented at the International Conference on Acoustic, Speech, and Signal Processing (ICASSP) 2008 and 2009. The associate editor coordinating the review of this manuscript and approving it for publication was Dr. Srdjan Stankovic.

The authors are with the Department of Electrical Engineering, Amirkabir University of Technology, Tehran, Iran (e-mail: nimakhademi@aut.ac.ir; sma@aut.ac.ir).

Color versions of one or more of the figures in this paper are available online at http://ieeexplore.ieee.org.

Digital Object Identifier 10.1109/TIP.2010.2042646

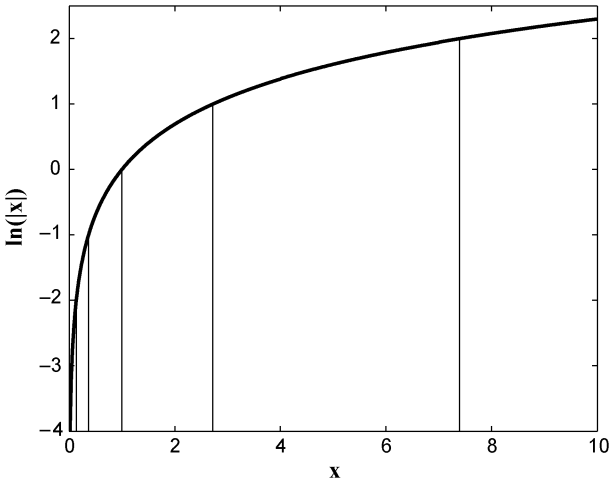

Fig. 1. $\ln(|x|)$ versus x. Quantizer points are shown in the original domain.

sizes is beneficial. However, the method proposed in [5] suffers from several drawbacks. Fig. 1 shows the logarithm function and the nonuniform step sizes in the original domain. As seen, the step sizes decrease by decreasing x which will result in very small step sizes for small x values. Although this characteristic is desirable from perceptual perspective, it is not efficient for data extraction in noisy environment. Due to very small step sizes for small amplitudes, there always exists error in detection even for low power attacks. Moreover, in the case where the original signal is zero, since the logarithm of zero is undefined, error exists in detection in the absence of any attacks. Furthermore, this function has not any freedom for controlling the distortion in fixed step sizes and the distortion cannot be minimized according to the host signal distribution. Finally, the perceptual advantages of this method are limited for some cases, e.g., quantizing DC coefficients in image, the large step sizes for coefficients with large values, leads to image pixelation effect.

Unfortunately, obtaining optimum quantizer levels is rather hard in general. Furthermore, implementation of such a quantization scheme is difficult and needs an exhaustive search through quantization levels. Moreover, optimum quantization is not necessarily perceptually advantageous. In this paper, inspired by a standard usually used in the processing of speech signals called μ-Law [11], we propose a Logarithmic QIM (LQIM) scheme which mitigates the aforementioned drawbacks of the proposed method in [5]. Here, the host signal features are transformed using a logarithmic function and then quantized uniformly regarding the watermark data. The watermarked data is obtained by applying inverse transform to the quantized data. Euclidean distance decoder is used to extract the watermark data. Also, the optimum μ, which results in minimum quantization distortion, is obtained analytically according to the host signal distribution. Using the proposed method, a host-dependent watermark will be obtained. Also, as a result of introducing host-dependent watermark, stronger watermark data can be inserted by LQIM in comparison with Uniform QIM (UQIM) with similar perceptual quality of watermarked data. Moreover, all the aforementioned drawbacks of [5] are solved using the controlling parameter μ which allows us to change the shape of the logarithm function. As it will be shown, using μ-Law compression function, step size decrements near zero amplitude are in control. In addition, this method is investigated in N-dimensional case by quantizing the magnitude of host vectors. For this, we use the surface of hyperspheres with logarithmic radii as our quantization codebooks. Distortion in this case is also minimized by calculating the optimum μ. The probability of error is derived for the proposed scheme by considering the host signal to follow Generalized Gaussian Distribution (GGD). The validity of analytical derivations is verified by simulations. Furthermore, data hiding using secret key is proposed and the probability of error in this case is also derived. Simulation results show the outstanding robustness of the proposed scheme in comparison with previous quantization-based algorithms.

This paper is organized as follows. Section II is devoted to proposing LQIM in scalar and vector cases. Then, optimum parameter finding is described in Section III. Host signal modeling and derivation of the probability of error is performed in Section IV. Section V explains data hiding using the secret key. Experimental results on real and artificial signals are investigated in Section VI. Finally, Section VII concludes the paper.

II. Logarithmic Quantization Index Modulation

μ-Law is a well-known concept, widely used in processing of speech signals to compress the amplitude of the speech signal in order to use less bits while keeping the quality of compressed speech at high level. Inspired by the μ-Law concept, we propose a logarithmic quantization by which stronger watermark can be inserted that introduces less distortion to the host signal. The rationale behind the logarithmic quantization is that since signal's amplitudes are more concentrated around zero, more step sizes should be devoted to quantizing smaller amplitudes and less should be associated to the larger amplitudes. This also leads to a more uniform signal-to-quantization error ratio for different amplitudes.

A. Scalar LQIM

In order to perform logarithmic quantization, the host signal must be transformed using the following compression function:

$$c = \frac{\ln\left(1+\mu\frac{|x|}{X_s}\right)}{\ln(1+\mu)}, \quad \mu > 0, X_s > 0 \tag{1}$$

where μ is a parameter defining the compression level and X_s is the parameter that scales the host signal. The best X_s value is the value which spreads most of the host signal samples into the range [0, 1]. The values that are larger than one can be converted to the logarithmic domain and be used for embedding. The function used in mu-law does not perform well for these values. Meanwhile, there exists only a small number of such values, and, thus, there is no major problem with them. In this regard, for artificial signals, we select X_s according to the signal model and in a way that the probability of occurrence of the host signal samples in the range $[-X_s, X_s]$ be sufficiently close to 1. Also, for real data, since the host signal samples (or features) may be inappropriately large, X_s should be carefully selected according to the histogram in a way that the host signal samples spread well into the range [0, 1]. The compression function for

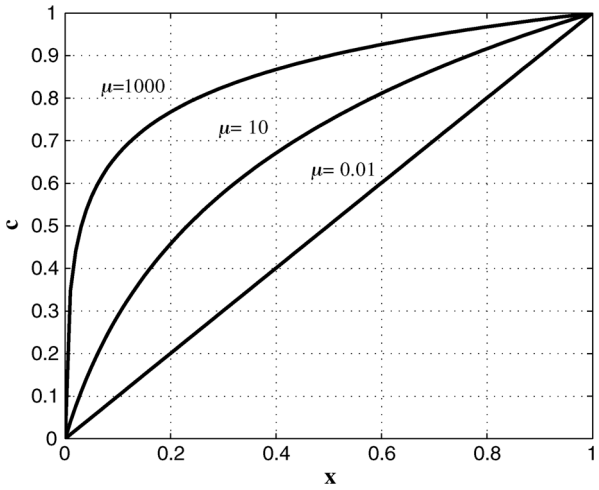

Fig. 2. c versus x according to equation (1) for different μ values.

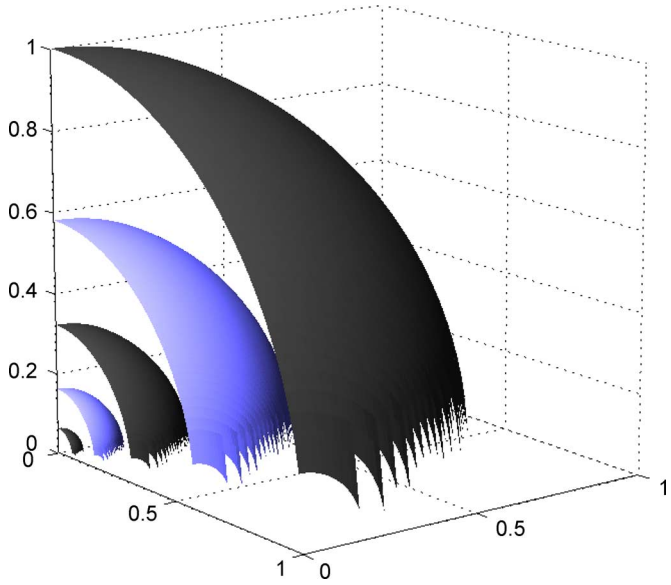

Fig. 3. Reconstruction areas in VQIM method. For better presentation, only one eighth of each sphere is shown. The surfaces with the same color belong to the same quantizer set.

different μ values is depicted in Fig. 2. As seen, identity function is obtained when μ becomes small. Furthermore, it is worth mentioning that when μ tends toward infinity, the compression function reduces to a logarithm function similar to that used in [5]. According to (1), when μ becomes small, using the approximation $\ln(1+x) \approx x$, we will have $c \approx |x|/X_s$ which is the identity function. Also when μ becomes large enough, 1 can be neglected in comparison with μ and for $|x| \gg X_s/\mu$ the compression function reduces to $c = 1 + \ln(|x|/X_s)/\ln(\mu)$.

The transformed signal is then used for data embedding. In this regard, the transformed signal is quantized uniformly regarding the watermark data similar to the UQIM [1]. The quantized data is then expanded, in order to obtain the watermarked signal, as follows:

$$x_w = \mathrm{sgn}(x)\frac{X_s}{\mu}\left[(1+\mu)^z - 1\right] \tag{2}$$

where $\mathrm{sgn}(\cdot)$ is the sign function, z is the quantized signal in the transformed domain, and x_w is the watermarked signal. In order to extract the watermark data, the Euclidean distance decoder is used. Euclidean distance decoder can be implemented in the original or the transformed domain. We found, both analytically and experimentally, as will be shown in Section VI-A, that the implementation in the original domain results in better robustness. In this regard, zero and one are embedded in the received signal (r) using the proposed method resulting in r_0 and r_1, respectively. The watermark data can be extracted by the following equation:

$$\hat{m} = \arg\min_{i\in\{0,1\}} \|r - r_i\|^2 \tag{3}$$

where $\hat{m}$ is the extracted watermark data. Note that here, exhaustive search through quantization levels is not needed, since we obtain the neighboring quantizer (r_0 and r_1) and then use (3) to find the closer neighbor. Thus, the extraction process remains simple. Decoder needs μ, X_s and quantization step size Δ to extract the watermark data. Other decoders such as Maximum Likelihood decoder can also be used to extract data, but the one proposed here is a simpler one.

Using this approach, the previously mentioned drawbacks of the method presented in [5] are addressed. According to Fig. 2, as c is limited to the range [0, 1], the step sizes for small amplitudes are in control. Moreover, since μ controls the shape of the logarithmic function, the introduced distortion can be optimized according to the host signal distribution which is investigated in Section III. Furthermore, as described before, by changing μ, the function can even be converted into the identity function, and, thus, it features improved perceptual advantages in comparison with the method of [5].

B. Vector LQIM

The proposed method can be generalized to N-dimensional space. For this, the magnitude of an N-dimensional vector is quantized using the proposed method. Fig. 3 demonstrates the quantization surfaces for embedding one and zero when $N = 3$. As seen, the surface of each sphere is our reconstruction area instead of the reconstruction point in scalar LQIM. Each vector, in order to lie on the surface of a sphere or a hypersphere, is moved according to the watermark data either upward or downward on the line connecting origin to it.

The described method can be implemented as simple as scalar LQIM. Consider $X = \{x_1, x_2, \cdots, x_N\}$ is the host signal vector. Our goal is to embed one bit of message into the whole vector. For this, the normalized magnitude is calculated as

$$s = \sqrt{\frac{1}{N}\sum_{i=1}^{N} x_i^2}. \tag{4}$$

Then using (1) and (2), s is quantized, which results in s_q. Each sample in the host signal vector is updated in a way that the magnitude of the vector be equal to s_q, i.e.,

$$X_w = \frac{s_q}{s}X \tag{5}$$

where X_w is the watermarked vector. Note that since $s = |x|$ when $N = 1$, this can be considered as the generalization of scalar LQIM to the vector case. Watermark data can also be extracted using minimum distance decoder, similar to scalar LQIM. The only difference is that for vector LQIM normalized magnitude of the received signal according to (4) should be used.

III. Optimum Parameter Finding

In this section, the optimum value for μ is found by minimizing the quantization distortion. It should be noted that μ can be found based on different metrics and this is only a suggestion for choosing μ. As an alternative, it can be obtained in a way to minimize the probability of error in a fixed perceptual quality, which is a good direction for future research. Since vector LQIM is a generalization of scalar method, we first describe the optimization for vector LQIM and then write down equations for scalar LQIM.

A. Vector LQIM (large N)

In order to obtain the optimum value for μ, we should find the watermark power and then minimize it with respect to μ. Consider the quantization noise in the transform domain to be w. Thus, we have $z = c + w$. In order to obtain the watermark power, we need to find $\mathrm{E}[\|x_w - x\|^2]$. According to (5), we have

$$x_w - x = \frac{s_q}{s}x - x = \left(\frac{s_q}{s} - 1\right)x. \tag{6}$$

In order to find $x_w - x$, s_q must be found first. Replacing z by $c + w$ in (2), we get

$$s_q = \frac{X_s}{\mu}\left[(1+\mu)^{c+w} - 1\right] \tag{7}$$

where $\mathrm{sgn}(s)$ is not considered, since s is always positive. By adding and subtracting $(1+\mu)^w$ inside the bracket and using (2), we have

$$s_q = s(1+\mu)^w + \frac{X_s}{\mu}\left[(1+\mu)^w - 1\right]. \tag{8}$$

Thus, $x_w - x$ can be obtained as

$$x_w - x = \left\{(1+\mu)^w + \frac{X_s}{s\mu}\left[(1+\mu)^w - 1\right] - 1\right\}x. \tag{9}$$

Simplifying the above equation leads to

$$x_w - x = \left(1 + \frac{X_s}{s\mu}\right)\left[(1+\mu)^w - 1\right]x. \tag{10}$$

From the above equation, $\mathrm{E}[\|x_w - x\|^2]$ can be found as

$$\mathrm{E}\left[\|x_w - x\|^2\right] = \mathrm{E}\left[\left(1+\frac{X_s}{s\mu}\right)^2\right]\mathrm{E}\left[\left((1+\mu)^w - 1\right)^2\right]\mathrm{E}[x^2]. \tag{11}$$

In (11), three terms inside the expectations have been considered as independent which is a correct assumption for sufficiently large N. Simulation results provided in Section VI-A prove our claim. For the first term, we have

$$\mathrm{E}\left[\left(1 + \frac{X_s}{s\mu}\right)^2\right] = 1 + 2\mathrm{E}\left[\frac{1}{s}\right]\frac{X_s}{\mu} + \mathrm{E}\left[\frac{1}{s^2}\right]\frac{X_s^2}{\mu^2} \tag{12}$$

where $\mathrm{E}[1/s]$ and $\mathrm{E}[1/s^2]$ should be calculated according to the host signal model. However, for very large N, these expectations can be approximated as $\mathrm{E}[1/s] \approx 1/\sigma_x$ and $\mathrm{E}[1/s^2] \approx 1/\sigma_x^2$. According to the Bennett's high-rate model for quantization noise, quantization noise, w, is considered to follow uniform distribution between $[-\Delta/2, \Delta/2]$, provided Δ is small, where Δ is the quantization step size. Therefore, we have

$$\mathrm{E}\left[\left((1+\mu)^w - 1\right)^2\right] = \frac{1}{\Delta}\int_{-\Delta/2}^{\Delta/2}\left((1+\mu)^w - 1\right)^2 dw \tag{13}$$

where, in order to save space, we have written the compact form rather than its closed form. By replacing the resultant expectations into (11), the watermark power is obtained. The optimum value for μ will be obtained by finding the derivative of the watermark power with respect to μ and equating the result to zero, which can be found numerically.

According to the obtained watermark power, Document to Watermark Ratio (DWR) can be calculated as

$$\mathrm{DWR} = \frac{\mathrm{E}\left[\|x\|^2\right]}{\mathrm{E}\left[\|x_w - x\|^2\right]} = \left\{\left(1 + 2\mathrm{E}\left[\frac{1}{s}\right]\frac{X_s}{\mu} + \mathrm{E}\left[\frac{1}{s^2}\right]\frac{X_s^2}{\mu^2}\right) \times \left(\frac{1}{\Delta}\int_{-\Delta/2}^{\Delta/2}\left((1+\mu)^w - 1\right)^2 dw\right)\right\}^{-1}. \tag{14}$$

As seen, when μ becomes large, the terms $\mathrm{E}[1/s^2]X_s^2/\mu^2$ and $\mathrm{E}[1/s]X_s/\mu$ can be neglected with respect to 1, and, thus, DWR will be independent of the host signal variance which leads to a watermark power proportional to the host signal power, similar to the proposed method in [5].

B. Scalar LQIM

The same analysis can be performed for scalar LQIM. Replacing s with $|x|$ in (10) and bringing x in the first parenthesis, we have

$$x_w - x = \left(x + \mathrm{sgn}(x)\frac{X_s}{\mu}\right)\left[(1+\mu)^w - 1\right] \tag{15}$$

where we have used $\mathrm{sgn}(x) = x/|x|$. Using (15), $\mathrm{E}[\|x_w - x\|^2]$ can be written as

$$\mathrm{E}\left[\|x_w - x\|^2\right] = \mathrm{E}\left[\left(x + \mathrm{sgn}(x)\frac{X_s}{\mu}\right)^2\right]\mathrm{E}\left[\left((1+\mu)^w - 1\right)^2\right]. \tag{16}$$

Again, two terms are assumed to be independent. For the first term, we have

$$\mathrm{E}\left[\left(x+\mathrm{sgn}(x)\frac{X_s}{\mu}\right)^2\right]=\mathrm{E}[x^2]+2\mathrm{E}\left[|x|\right]\frac{X_s}{\mu}+\frac{X_s^2}{\mu^2}. \quad (17)$$

The watermark power can be calculated using (17). The watermark power can be minimized with respect to μ using the same approach used in vector LQIM. DWR, in this case, can also be obtained as follows:

$$\mathrm{DWR}=\left\{\left(1+2\mathrm{E}\left[|x|\right]\frac{X_s}{\mathrm{E}[x^2]\mu}+\frac{X_s^2}{\mathrm{E}[x^2]\mu^2}\right)\times\left(\frac{1}{\Delta}\int_{-\Delta/2}^{\Delta/2}\left((1+\mu)^w-1\right)^2dw\right)\right\}^{-1}. \quad (18)$$

C. Low Watermark Power

For perceptual reasons, the watermark power should be low. This is essential since we do not want to introduce much distortion to the host signal. Consequently, quantization distortion should be low, and, thus, in some cases, quantization step size Δ should be small. Therefore, by writing the Taylor series expansion for $(1+\mu)^w$ in (13), we have

$$(1+\mu)^w=1+\ln(1+\mu)w+O(2)$$

where we have neglected the higher order terms by assuming Δ to be sufficiently small. Using the above approximation, we can obtain the expectation in (13) as

$$\mathrm{E}\left[\left((1+\mu)^w-1\right)^2\right]=\ln^2(1+\mu)\frac{\Delta^2}{12}.$$

Using the above simplification, the optimum μ can be found for scalar LQIM as follows:

$$\mu_o=\arg\min_{\mu\in(0,\infty)}\left\{\left(1+\frac{2\mathrm{E}\left[|x|\right]X_s}{\mathrm{E}[x^2]\mu}+\frac{X_s^2}{\mathrm{E}[x^2]\mu^2}\right)\ln^2(1+\mu)\right\}. \quad (19)$$

Also for vector LQIM, μ_o can be found as

$$\mu_o=\arg\min_{\mu\in(0,\infty)}\left\{\left(1+2\mathrm{E}\left[\frac{1}{s}\right]\frac{X_s}{\mu}+\mathrm{E}\left[\frac{1}{s^2}\right]\frac{X_s^2}{\mu^2}\right)\ln^2(1+\mu)\right\}. \quad (20)$$

As seen from (19) and (20), optimization is independent of quantization step size when the watermark power is low.

IV. Derivation of Bit Error Probability

Generalized Gaussian Distribution (GGD) has been used for modeling transform domain, such as Discrete Wavelet Transform (DWT) and Discrete Cosine Transform (DCT) [12]–[14]. Thus, for the sake of generality, the original signal is modeled by a GGD which is defined as

$$f_x(x;\mu,\sigma,\nu)=\frac{1}{2\Gamma\left(1+\frac{1}{\nu}\right)A(\nu,\sigma)}e^{-\left|\frac{x-\mu}{A(\nu,\sigma)}\right|^\nu} \quad (21)$$

where μ is the mean of the distribution, which we considered to be zero, σ is its standard deviation, ν is the shape parameter which determines the exponential rate of decay, $\Gamma(\cdot)$ is the gamma function and $A(\nu,\sigma)$ is defined as follows:

$$A(\nu,\sigma)=\sqrt{\frac{\sigma^2\Gamma(1/\nu)}{\Gamma(3/\nu)}}.$$

When $\nu=1$, the GGD corresponds to a Laplacian distribution and if $\nu=2$ it corresponds to a Gaussian distribution. σ for GGD can be estimated from observations with Maximum Likelihood (ML) method [15] as

$$\hat{\sigma}=\left[\frac{\Gamma(3/\nu)}{\Gamma(1/\nu)}\right]^{1/2}\left(\frac{\nu}{N}\sum_{i=1}^{N}x_i^\nu\right)^{1/\nu}. \quad (22)$$

The shape parameter (ν) is estimated using the method of moments, as follows [15]:

$$\nu=F^{-1}(\xi),\quad \xi=\frac{\mathrm{E}\left(|x|\right)}{\sqrt{\mathrm{E}(x^2)}}$$
$$F(\xi)=\frac{\Gamma(2/\xi)}{\sqrt{\Gamma(1/\xi)\Gamma(3/\xi)}}. \quad (23)$$

A. Scalar LQIM

We conduct the analysis by considering the watermarked signal to be sent through an Additive White Gaussian Noise (AWGN) channel, i.e., $r=x_w+n$. Error in detection occurs when noise causes the received signal to fall into a wrong region. Thus, the probability of error can be obtained as follows:

$$P_e=\sum_{i=-\infty}^{\infty}o_i\sum_{m=-\infty}^{\infty}\int_{T_{i+2m}}^{T_{i+1+2m}}\frac{1}{\sqrt{2\pi}\sigma_n}\mathrm{e}^{\frac{(n-C_{i/2})^2}{2\sigma_n^2}}dn \quad (24)$$

where σ_n^2 is the noise variance, T_i is defined as

$$T_i=\frac{C_{i/2}+C_{(i+1)/2}}{2}$$

and o_i is the probability of occurrence of the host signal in the interval $[C_{(i-1)/2},C_{(i+1)/2}]$, which by assuming equal probabilities for zero and one bits, is defined as

$$o_i=\frac{1}{2}\int_{C_{(i-1)/2}}^{C_{(i+1)/2}}\frac{1}{2\Gamma\left(1+\frac{1}{\nu}\right)A(\nu,\sigma)}e^{-\left|\frac{x}{A(\nu,\sigma)}\right|^\nu}dx \quad (25)$$

where C_i is

$$C_i=\mathrm{sgn}(i)\frac{X_s}{\mu}\left[(1+\mu)^{(|i\Delta|)}-1\right].$$

B. Vector LQIM

In the decoder side, the normalized magnitude of the received signal is calculated as follows:

$$s_r = \sqrt{\frac{1}{N}\sum_{i=1}^{N}(x_{w_i}+n_i)^2}. \tag{26}$$

Since s_r is not easy to handle, we continue our analysis using s_r^2. Decomposing s_r^2, we have

$$s_r^2 = \frac{1}{N}\sum_{i=1}^{N}\left(x_{w_i}^2 + 2x_{w_i}n_i + n_i^2\right) \tag{27}$$

The above equation can be divided into clean and noisy terms, i.e., $s_r^2 = s_q^2 + n_v$, where $s_q^2 = 1/N\sum_{i=1}^{N}(x_{w_i}^2)$ is the clean term and $n_v = 1/N\sum_{i=1}^{N}(2x_{w_i}n_i + n_i^2)$ is the noisy term. Here, error in detection occurs when noisy term causes the clean term to fall into a wrong region. In order to calculate the probability of error we should find the probability distribution function (pdf) of n_v. In obtaining the distribution of n_v, we assume that the host signal's vector dimension (N) is sufficiently large to use the Central Limit Theorem (CLT). Using CLT we can model the first and second terms of n_v with Gaussian distributions as follows:

$$\frac{1}{N}\sum_{i=1}^{N}n_i^2 \sim \mathcal{N}\left(\sigma_n^2, \frac{2\sigma_n^4}{N}\right) \tag{28}$$

$$\frac{1}{N}\sum_{i=1}^{N}x_i n_i \sim \mathcal{N}\left(0, \frac{\sigma_{x_q}^2\sigma_n^2}{N}\right) \tag{29}$$

where $\sigma_{x_q}^2$ is the variance of the watermarked host signal vector for which s_r^2 is calculated. Note that $\sum n_i^2$ has a positive value, whereas it has been modeled with a Gaussian distribution in (28). The probability that $\mathcal{N}(\sigma_n^2, (2\sigma_n^4/N))$ becomes negative is equal to $\Phi(-\sqrt{N/2})$ which depends on the number of samples in each subset N. For example, when $N = 32$ this value is approximately 3.16×10^{-5} which can be neglected. Thus, the distribution of n_v can be easily found using the obtained distributions as

$$n_v \sim \mathcal{N}\left(\mu_{n_v}, \sigma_{n_v}^2\right) = \mathcal{N}\left(\sigma_n^2, \frac{4\sigma_{x_q}^2\sigma_n^2 + 2\sigma_n^4}{N}\right). \tag{30}$$

where the first and second parts of noisy term are assumed to be independent which we found through simulations. For this, we considered $\sigma_x^2 = 1$, $\sigma_n^2 = 1/8$, and $N = 30$, and compared the empirical cdf of n_v with the analytical one, given in (30). Comparison showed that maximum difference of the empirical and analytical cdfs in this case is about 0.02 which shows the accuracy of (30). Also, the probability of error can be obtained as

$$P_e = \sum_{i=0}^{\infty}o_i' \sum_{m=-\lfloor i/2\rfloor}^{\infty}\int_{T_{i+2m}^2}^{T_{i+1+2m}^2}\frac{1}{\sqrt{2\pi}\sigma_{n_v}}\mathrm{e}^{\frac{\left(n-\mu_{n_v}-C_{i/2}^2\right)^2}{2\sigma_{n_v}^2}}dn \tag{31}$$

where $\lfloor\cdot\rfloor$ refers to the floor function and $T(-1)$ should be set equal to zero. Here, C^2 and T^2 are used since we performed the analysis using s_r^2. Furthermore, o_i' is the probability of occurrence of s^2 in the interval $[C_{(i-1)/2}^2, C_{(i+1)/2}^2]$. In order to calculate this probability, pdf of s^2 should be found. Again assuming N to be sufficiently large, we can use CLT to obtain the distribution function of s^2. However, this is not a good approximation when ν is much smaller than 2. In order to model s^2 with Gaussian distribution, we should find the mean and variance of x_i^2. According to [15], central moment for GGD is

$$\mathrm{E}\left[|x|^r\right] = \left[\frac{\sigma_x^2\Gamma(1/\nu)}{\Gamma(3/\nu)}\right]^{r/2}\frac{\Gamma\left(\frac{r+1}{\nu}\right)}{\Gamma(1/\nu)}. \tag{32}$$

Therefore, we have

$$\begin{aligned}\mathrm{E}\left[|x_i|^2\right] &= \sigma_x^2,\\ \mathrm{var}\left(x_i^2\right) &= \mathrm{E}\left[|x_i|^4\right] - \left(\mathrm{E}\left[|x_i|^2\right]\right)^2\\ &= \sigma_x^4\left[\left(\frac{\Gamma(1/\nu)\Gamma(5/\nu)}{\Gamma^2(3/\nu)}\right) - 1\right].\end{aligned} \tag{33}$$

Using mean and variance of x_i^2, the pdf of s^2 can be obtained as

$$f_s(s^2) = \mathcal{N}\left(\mu_s, \sigma_s^2\right) \tag{34}$$

where

$$\mu_s = \sigma_x^2, \quad \sigma_s^2 = \frac{\sigma_x^4}{N}\left[\left(\frac{\Gamma(1/p)\Gamma(5/p)}{\Gamma^2(3/p)}\right) - 1\right].$$

Thus, by assuming equal probabilities for zero and one bits, o_i' is defined as

$$o_i' = \frac{1}{2}\int_{C_{(i-1)/2}^2}^{C_{(i+1)/2}^2}\frac{1}{\sqrt{2\pi}\sigma_s}\mathrm{e}^{\frac{(s-\mu_s)^2}{2\sigma_s^2}}ds, \quad i \geq 1. \tag{35}$$

Since s^2 is positive, o_0' is obtained using the above equation and integrating from 0 to $C_{1/2}^2$. Note that $\sigma_{x_q}^2$, in (30), is not the variance of host signal and should be calculated according to the same watermarked host signal vector. For large N, s_q^2 is a reliable estimation of $\sigma_{x_q}^2$. Thus, we have

$$\sigma_x^2 = s_q^2 = C_{i/2}^2. \tag{36}$$

From (30), it is obvious that by increasing N, variance of the noisy term and consequently error in detection is reduced. Moreover, the noisy term has a mean which results in more error in detection. In the case where the noise variance can be estimated, it can be subtracted from s_r^2, which results in better decoder performance. This effect is thoroughly investigated in Section VI-A.

V. Data Hiding With Secret Key

The proposed method is not secure since attackers can find the embedding pattern using the histogram of the watermarked signal and extract the watermark signal. In order to make the proposed method secure, we need to use a secret key for data hiding. Here, we cannot use dithering as used in [1] and [5], since shifting the quantizer levels using a random key may result in negative quantizer levels which are not acceptable in our method. Thus, we use μ for shifting the quantizer levels. In this

regard, μ can be selected randomly (e.g., with uniform distribution) around its optimum value in the interval $[\mu_o - d_1, \mu_o + d_2]$ where d_1 and d_2 define the deviation of the μ from its optimum value from left and right sides respectively. As seen, the interval around μ_o can be asymmetric. These values will be sent to the receiver side as a secret key to be used for watermark extraction. In this manner, an attacker cannot find the quantization pattern due to the random location of quantization levels. The size of interval of these values around the optimum value depends on the level of security a system desires. As will be discussed in Section VI-A, using random μ does not substantially affect the quality of watermarked data and bit error probability. DWR of the watermarked data, for scalar LQIM, can be obtained as

$$\mathrm{DWR} = \int_{\mu_o - d_1}^{\mu_o + d_2} f_\mu(\mu) \left\{ \left(1 + 2\mathrm{E}\left[|x|\right] \frac{X_s}{\mathrm{E}[x^2]\mu} + \frac{X_s^2}{\mathrm{E}[x^2]\mu^2} \right) \times \mathrm{E}\left[\left((1+\mu)^w - 1 \right)^2 \right] \right\}^{-1} d\mu \quad (37)$$

where $f_\mu(\mu)$ is the distribution of μ, and μ_o is the optimum μ. Also the probability of error in this case is

$$P_e = \int_{\mu_o - d_1}^{\mu_o + d_2} f_\mu(\mu) \left(\sum_{i=-\infty}^{\infty} o_i \sum_{m=-\infty}^{\infty} \times \int_{T_{i+2m}}^{T_{i+1+2m}} \frac{1}{\sqrt{2\pi}\sigma_n} \mathrm{e}^{\frac{(n - C_{i/2})^2}{2\sigma_n^2}} dn \right) d\mu. \quad (38)$$

Also for vector LQIM, we have

$$\mathrm{DWR} = \int_{\mu_o - d_1}^{\mu_o + d_2} f_\mu(\mu) \times \left\{ \left(1 + 2\mathrm{E}\left[\frac{1}{s}\right] \frac{X_s}{\mu} + \mathrm{E}\left[\frac{1}{s^2}\right] \frac{X_s^2}{\mu^2} \right) \times \mathrm{E}\left[\left((1+\mu)^w - 1 \right)^2 \right] \right\}^{-1} d\mu \quad (39)$$

$$P_e = \int_{\mu_o - d_1}^{\mu_o + d_2} f_\mu(\mu) \times \left(\sum_{i=0}^{\infty} o_i' \sum_{m=-\lfloor i/2 \rfloor}^{\infty} \int_{T_{i+2m}^2}^{T_{i+1+2m}^2} \times \frac{1}{\sqrt{2\pi}\sigma_{n_v}} \mathrm{e}^{\frac{\left(n - \mu_{n_v} - C_{i/2}^2\right)^2}{2\sigma_{n_v}^2}} dn \right) d\mu. \quad (40)$$

A. Choosing appropriate interval for μ

In order to have a completely secure system, d_1 and d_2 should be chosen carefully. The method is secure when an attacker cannot estimate the quantizer levels from the histogram of watermarked signal. Therefore, these values should be selected in a way that there would not be any discontinuity in the histogram. The watermarked signal has continuous histogram when the following equations are satisfied:

$$\begin{aligned} &\frac{X_s}{\mu_o - d_1} \left[(1 + \mu_o - d_1)^{\frac{i\Delta}{2}} - 1 \right] \\ &\quad = \frac{X_s}{\mu_o} \left[(1 + \mu_o)^{\frac{(2i+1)\Delta}{4}} - 1 \right] \\ &\frac{X_s}{\mu_o + d_2} \left[(1 + \mu_o + d_2)^{\frac{(i+1)\Delta}{2}} - 1 \right] \\ &\quad = \frac{X_s}{\mu_o} \left[(1 + \mu_o)^{\frac{(2i+1)\Delta}{4}} - 1 \right]. \end{aligned} \quad (41)$$

These equations have been found according to the fact that in order to make the histogram continuous, the gap between two quantizer levels should be filled. This is carried out by equating the values of the quantization level found using $\mu_o - d_1$ and the next quantization level found using $\mu_o + d_2$. As seen, both equations are functions of i. Thus, the desired value for d_1 and d_2 should be the maximum values obtained from solving (41) by changing i. The obtained values for d_1 and d_2 decrease when i increases. Thus, the above equations should be solved for $i = 1$. Due to the usage of μ-law rule, the quantizer level at zero is fixed for all μ values which results in a peak at zero for the histogram of the watermarked signal. However, this does not jeopardize the security of system since an attacker cannot extract all bits from the zero quantizer level. Furthermore, it does not introduce much distortion, as will be shown experimentally and analytically in Section VI-A.

Again here, (41) can be simplified assuming the small quantization step size. Using Taylor series expansion, the above equations are simplified to

$$\begin{aligned} \frac{\ln(1 + \mu_o - d_1)}{\mu_o - d_1} &= \frac{3\ln(1 + \mu_o)}{2\mu_o} \\ \frac{\ln(1 + \mu_o + d_2)}{\mu_o + d_2} &= \frac{3\ln(1 + \mu_o)}{4\mu_o}. \end{aligned} \quad (42)$$

As can be seen, the μ interval is obtained independent of Δ and only depends on μ_o for small Δ.

VI. Experimental Results

In order to evaluate the performance of the proposed method and validity of analytical derivations, the proposed method is simulated on artificial and real signals. We first conduct the experiment by simulation on artificial signals to show the performance of scalar and vector LQIM in different situations. Then the method is simulated on real images to show its perceptual advantages in comparison with previous quantization-based methods.

A. Simulation on Artificial Signals

We generated an i.i.d. GGD random variable to be used as host signal to evaluate the performance of the proposed method and accuracy of analysis. For this, random values following GGD with $\sigma^2 = 1$ and $\nu = 1.5$ were generated to be used in all simulations of this section. Also, X_s was set equal to 4.7, which was calculated in a way that the probability of values larger than X_s or smaller than $-X_s$ be 10^{-4}. Overall, results were obtained

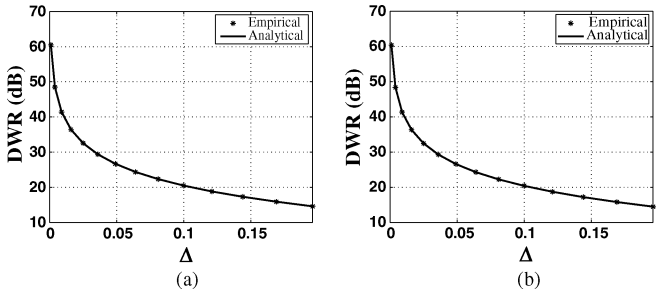

Fig. 4. Empirical and analytical DWR as a function of Δ for scalar LQIM (a) without using secret key (b) using secret key.

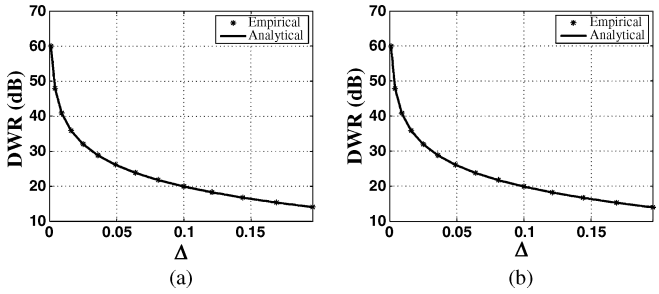

Fig. 5. Empirical and analytical DWR as a function of Δ for vector LQIM (a) without using secret key (b) using secret key.

by averaging the results over 50 simulations with 100000 bits each to ensure the accuracy of empirical results.

Fig. 4 demonstrates the empirical and analytical DWR for scalar LQIM with and without secret key. μ_o was calculated using the method proposed in Section III and was around 5.7 for all Δs. Furthermore, in implementing the scalar LQIM with secret key, d_1 and d_2 were found using the method in Section V. d_1 was in the range of [3.2, 3.7] and d_2 was in [3.6, 5.5].

Fig. 4(a) shows the empirical and analytical results of DWR for different quantization step sizes. As seen, the results agree well which confirms the accuracy of analysis provided in Section III. The effect of using secret key in this method is demonstrated in Fig. 4(b). As seen, the DWRs in this case are similar to the results in Fig. 4(a) and in worst case there was a 0.1 dB reduction in DWR value.

Fig. 5 shows the same results for vector LQIM. Here, each watermark bit was embedded in a host signal vector with 30 samples. μ_o was around 6 and the ranges of d_1 and d_2 were equal to [3.3, 3.8] and [3.8, 5.7], respectively. Fig. 5(a) shows the empirical and analytical DWRs as a function of quantization step size. As seen, the empirical and analytical results are once again very close. Moreover, the effect of using secret key in vector LQIM is investigated in Fig. 5(b). Here, similar to the scalar case, the DWR reduction as a result of using secret key is very small.

In order to support the claim made in Section II-A about better performance of Euclidean distance decoder in the original domain, the decoder was implemented in original and logarithmic domains. In this regard, DWR was fixed at 10 dB for better illustration of the differences in performance. Furthermore μ_o was found as 5.2. Each plot has been obtained in different Watermark to Noise Ratios (WNR), defined as follows:

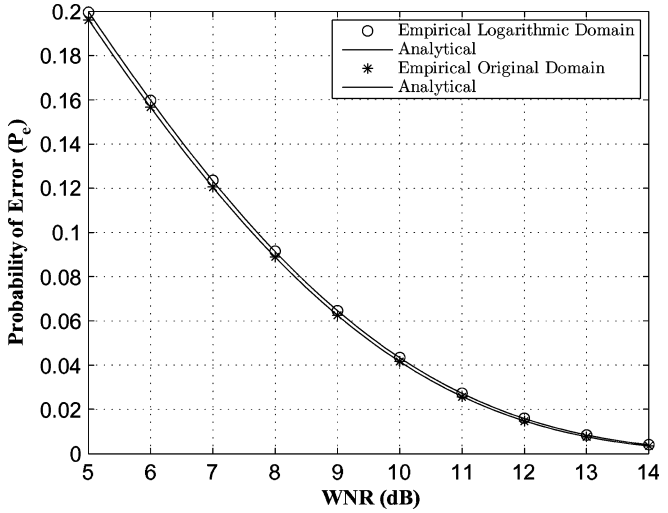

Fig. 6. Comparison of the performance of Euclidean distance decoder in the original and transformed domains ($\mathrm{DWR} = 10$ dB).

$$\mathrm{WNR} = 10 \log \frac{\mathrm{E}\left[\|x_{w_i} - x_i\|^2\right]}{\mathrm{E}\left[\|r_i - x_{w_i}\|^2\right]}. \tag{43}$$

where x_i is the host signal sample and x_{w_i} is the watermarked signal sample, and r_i is the received signal sample. Here, noise is assumed to be White Gaussian Noise (WGN). The results are shown in Fig. 6. Analytical probability of error for the decoding in the logarithmic domain was obtained using the equations in Section IV-A, except that here $T_i = C((2j+1)/4)$. As seen from empirical and analytical results, the performance of the decoder in the original domain is slightly better than the decoder in the logarithmic domain. This is due to the fact that in scalar LQIM, noise is Gaussian in the original domain. Thus, the best case is to set the middle of two quantization levels, as the separation point for zero and one regions. The same analysis is correct for vector LQIM since according to (30), noise is Gaussian in this case.

For evaluating the performance of the proposed method and validate the analytical prediction of the probability of error, implementation of secure and nonsecure methods were carried out using different N values. In this regard, Δ was chosen equal to 0.05 which results in DWR around 26 dB which is an average value. Furthermore, μ_o was found equal to 5.7 for the scalar case and 6 for the vector case. Also, for scalar LQIM using secret key, $d_1 = 3.3$ and $d_2 = 4$, and for vector LQIM, $d_1 = 3.4$ and $d_2 = 4.2$. Fig. 7 shows the performances of scalar and vector LQIM for different N values. The results for the scheme without and with secret key are demonstrated in Fig. 7(a) and (b), respectively. Comparing these figures, we can conclude that the probabilities of error in both cases are similar, which shows that using secret key does not degrade the performance of the proposed method. Furthermore, as seen, the system performance gets better with increasing N, which is obvious according to

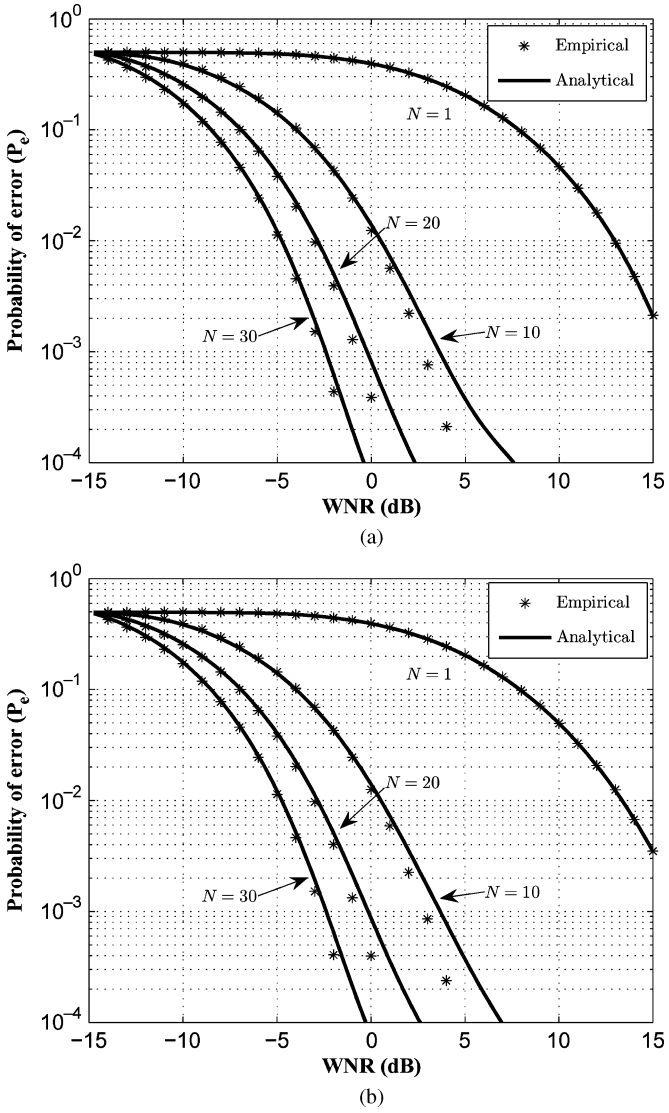

Fig. 7. Empirical and analytical probability of error for scalar LQIM and vector LQIM with different N values ($\mathrm{DWR} \approx 26$ dB): (a) nonsecure method; (b) secure method.

the noise modeling provided in (30). Moreover, the analytical and empirical results for scalar LQIM are very close. Also, for vector LQIM, as N increases, the empirical and analytical results get closer. This is due to the use of CLT in Section IV-B whose accuracy increases with larger N values.

Finally, we investigated the effect of noise subtraction in improving the performance of vector LQIM, as discussed in Section IV-B. According to (30), in order to reduce the probability of error, mean of n_v should be zero. In this regard, σ_n^2 should be subtracted from s_r^2. It should be noted that better improvement will be achieved when N is large. In this case, $1/N\sum_{i=1}^{N} n_i^2$ is a more accurate estimate of σ_n^2 and, thus, subtraction results in the removal of this term. Fig. 8 demonstrates the results for vector LQIM with $N = 30$ with and without using noise subtraction. As it is clear, the results using noise estimation is better, and, thus, it is better to use this scheme wherever noise variance estimation is possible.

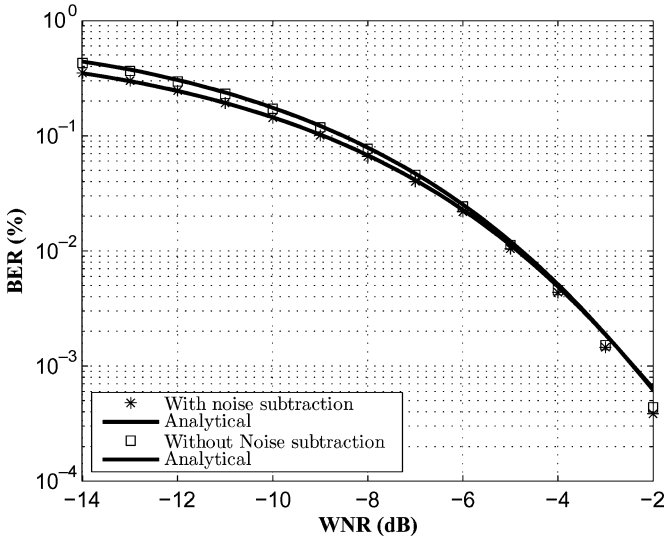

Fig. 8. Comparison of the performance of vector LQIM with and without noise subtraction ($N = 30$).

B. Simulation on Real Images

Here, we conduct experiments on real images to show the perceptual advantages of LQIM in comparison with previous quantization-based methods. The method was applied to different well-known images. However, in order to save space and be able to report all used parameters, the results are reported here for Lena image. The robustness of the proposed method under Additive Gaussian Noise attack on ten well-known images including Baboon, Barbara, F16, etc., is also investigated.

1) Scalar LQIM: LQIM, UQIM and the method proposed in [5] were implemented in the wavelet transform domain. For this, a three-level wavelet transform with HAAR filter was applied to the host image. Then, the diagonal detail coefficients of the third level were used for quantization, resulting in embedding of 4096 bits in a 512×512 host image. Parameters were selected for all methods in a way that perceptual quality of the watermarked images be similar. Since the watermarked images for all methods were so similar that it was very difficult to recognize their differences with subjective measures, we used Watson distance [18] as a metric to evaluate the quality of watermarked images. The Watson distance for all methods were around 100 to ensure invisibility of the watermark insertion. Δ was selected equal to 0.4, 36.5, and 1.4 for LQIM, UQIM, and [5], respectively. Moreover, for LQIM, we set $X_s = 240$ and μ_o was found according to the method described in Section III and was equal to 8.25.

The watermarked Lena images are depicted in Fig. 9 for UQIM and LQIM. As can be seen, the quality of both images is acceptable. Although the PSNR of the Watermarked image for UQIM is 45.6 dB and for LQIM is 42.3 dB, their Watson distances and perceptual qualities are similar. The differences of the original and watermarked images in a magnified form are shown for both methods in Fig. 10. Here, the differences were scaled into the range 0 to 255. As seen, LQIM provides image-dependent watermark which has strong components in the complex part of the image, which is hard to see. This

(a) (b)

Fig. 9. Watermarked Lena image using (a) UQIM and (b) LQIM methods.

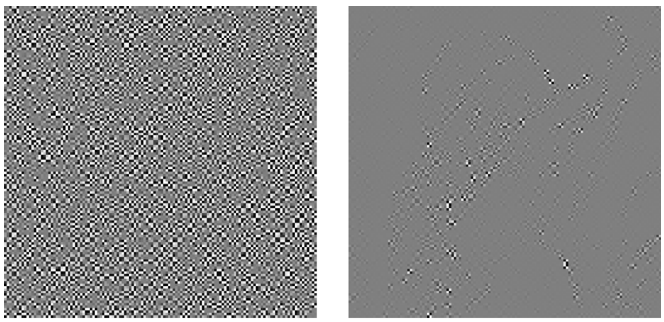

(a) (b)

Fig. 10. Scaled differences of the original and watermarked Lena images using (a) UQIM and (b) LQIM methods.

allows us to insert strong watermark whereas the perceptual quality of the watermarked image is kept at acceptable level, while uniform QIM embeds data uniformly in the whole image, which can be seen easily in the less textured part of the image. As an example, one can see the strong watermark components around feather and hat. Furthermore, PSNR for the method presented in [5] was 41.8. Although this method introduced stronger watermark, due to its aforementioned shortcomings, as will be discussed, it has not shown good performance against attacks.

Fig. 11 demonstrates the robustness of the LQIM in comparison with UQIM and [5] under AWGN attack. For better illustration, the results for some σ_n values are demonstrated in Table I. Regarding this figure and table, there are several comments in order. First, as can be seen, LQIM outperforms UQIM and [5]. However, LQIM has slightly larger Bit Error Rate (BER) in low attack power. This is due to smaller quantization step size for low amplitudes in LQIM method. Second, [5] has BER in the absence of any attacks. This is due to some zero coefficients for which log(0) is undefined. Finally, the BER of this method increases very fast as a result of very small step sizes for low amplitude coefficients. However, [5] features lower BER for high watermark power, in comparison with UQIM, as a result of larger step sizes for high amplitudes. Also, the analytical prediction and empirical results for LQIM are very close which shows that GGD models the wavelet coefficients well. Simulations were also performed on ten well-known images and the average results are depicted in Fig. 12. As seen, the same results are obtained on different images. Moreover robustness of

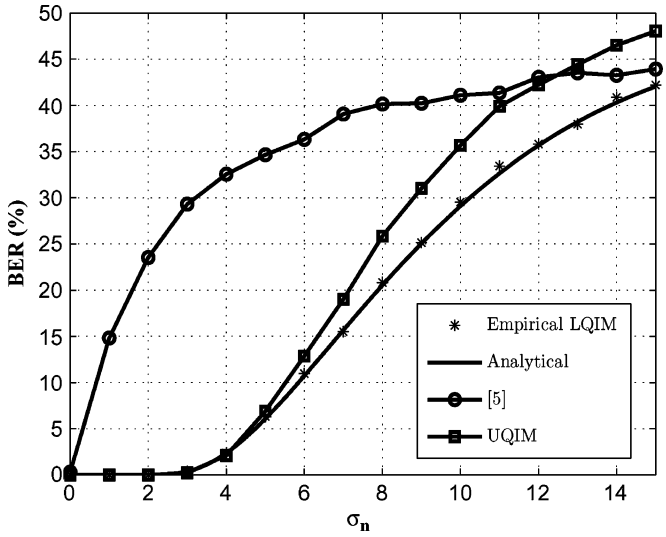

Fig. 11. BER (%) of watermark extraction under AWGN attack for various noise variances. 4096 bits have been embedded in Lena image in all methods.

TABLE I
RESULTS DEPICTED IN FIG. 11 FOR SOME σ_n VALUES

σ_n	BER (%)		
	LQIM	UQIM	[5]
0	0	0	0.3092
1	0	0	14.8193
2	0	0	23.5189
3	0.3988	0.2279	29.2969
4	2.36	2.1077	32.5602
5	6.3232	6.8929	34.6436
6	10.9619	12.8743	36.32

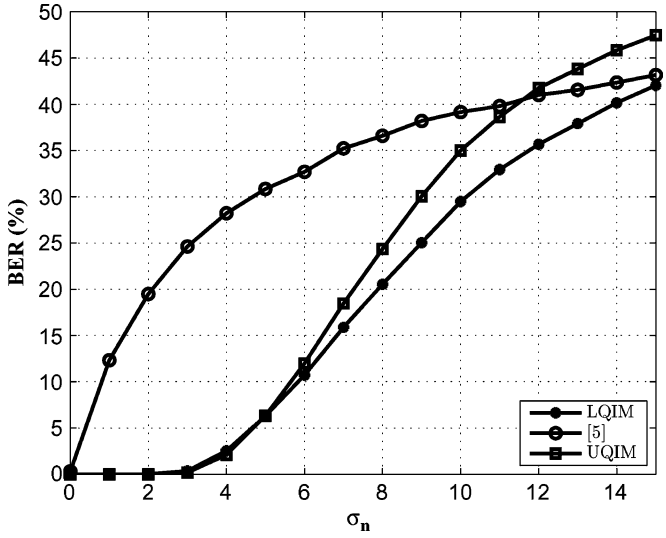

Fig. 12. BER (%) of watermark extraction under AWGN attack for various noise variances. The results are averaged over ten well-known images. 4096 bits have been embedded in each image in all methods.

all methods were tested under some common attacks and the results are depicted in Table II. As seen LQIM outperforms the other methods.

TABLE II
BER(%) OF WATERMARK EXTRACTION FOR SOME COMMON ATTACKS. 4096 BITS HAVE BEEN EMBEDDED IN LENA IMAGE IN ALL METHODS. THE WINDOW SIZE FOR GAUSSIAN FILTER IS 3×3

Attacks		BER (%)		
		LQIM	UQIM	[5]
Median filtering	3×3	10.58	13.14	31.29
Gaussian filtering	$\sigma^2 = 0.2$	0	0	0.21
	$\sigma^2 = 0.4$	0	0.02	4.19
	$\sigma^2 = 0.6$	0.77	5.2	16.9

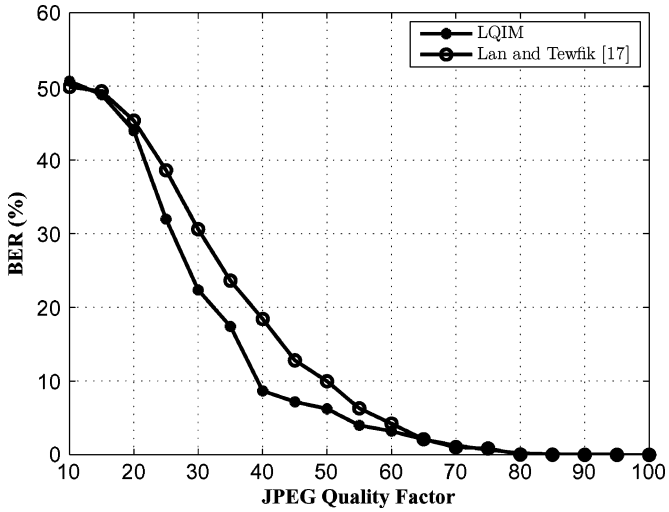

Fig. 13. BER(%) versus JPEG quality factor for JPEG compression attack. 4096 bits have been embedded in Lena image in all methods.

TABLE III
RESULTS DEPICTED IN FIG. 13 FOR SOME JPEG QUALITY FACTORS

JPEG quality factor	BER (%)		
	LQIM	UQIM	[5]
95	0	0	29.0625
85	0.1196	0.0117	30.043
75	0.5615	0.5103	31.2949
65	2.2969	1.8213	31.9546
55	3.5688	8.0981	33.04
45	3.5439	5.3291	34.8003

As one of the most common attacks, we also simulated all methods against JPEG compression attack. The results are depicted in Fig. 13 and for some JPEG quality factors in Table III. As seen, BER for LQIM in some high JPEG quality factors is slightly more than UQIM. Here, due to the aforementioned problems of [5], it has high BER even in high JPEG quality factors. However, similar to AWGN attack, it has better performance, in comparison with UQIM, in low JPEG quality factors.

Also, the proposed method was compared with a quantization-based method proposed in [17] and the results are shown in Fig. 14. In [17] STDM is used to embed data within a cover image in the DCT domain. In both methods, the three first components in the first row of the DCT coefficients, including DC and two AC coefficients, were used for data embedding, resulting in embedding of 12288 bits in the host image. The PSNR of [17] for Lena image was 45 dB and that of LQIM was 40 dB. Furthermore, the Watson distance for both methods was around

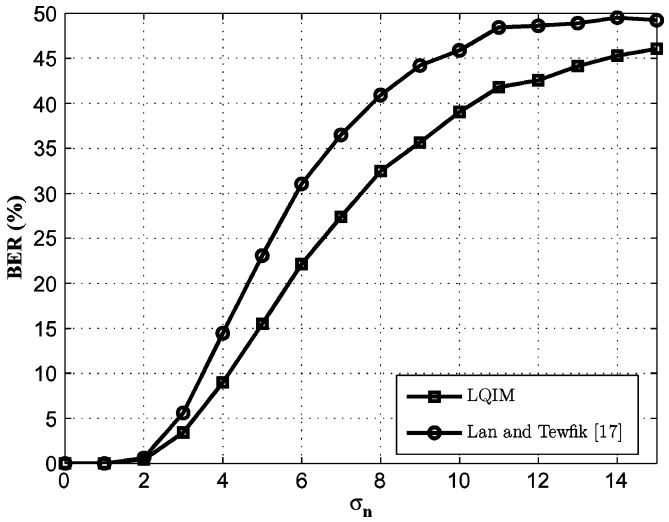

Fig. 14. BER (%) of watermark extraction under AWGN attack for various noise variances. 12288 bits have been embedded within Lena image in both methods.

TABLE IV
VALUE OF PARAMETERS FOR SCALAR LQIM USED FOR QUANTIZING THREE DCT COEFFICIENTS

Coefficients	Δ	X_s	μ_o
DC	0.015	1750	5
First AC	0.12	700	10.3
Second AC	0.27	320	10.1

215. The Δ values for the three coefficients were selected empirically in a way that resulted in similar perceptual quality with [17]. These values are summarized in Table IV. As seen in Fig. 14, due to inherent consideration of perceptual characteristic, our method shows a better robustness.

Furthermore, robustness of both methods under the JPEG compression attack was tested and results are demonstrated in Fig. 15. It is worth mentioning that although [17] is devised in a way to be robust against JPEG compression, LQIM is more robust than this method with the same capacity and perceptual quality.

2) Vector LQIM: The vector LQIM was also simulated and was compared with Sphere-Hardening Dither Modulation (SHDM) proposed in [19]. There, spherical codebooks are used similar to the method proposed in this paper. The only difference of SHDM with vector LQIM is that in SHDM uniform quantization is used. Both methods were implemented in the wavelet transform domain and a three-level wavelet transform with HAAR filter were applied to the host image. Again diagonal detail coefficients of third level, i.e., 4096 coefficients, were used for data embedding. Length of host vectors N for both methods were 32 which result in embedding 128 bits in the host image.

Parameters were set in a way that perceptual quality of both schemes be similar. In this regard, Δ for SHDM and vector LQIM was equal to 31 and 0.36, respectively. Furthermore, X_s was equal to 118 and μ_o was calculated as 1.7. PSNR for SHDM was 47.3 dB and for vector LQIM was equal to 45.7. Also watson distance for both method was equal to 45. BER of

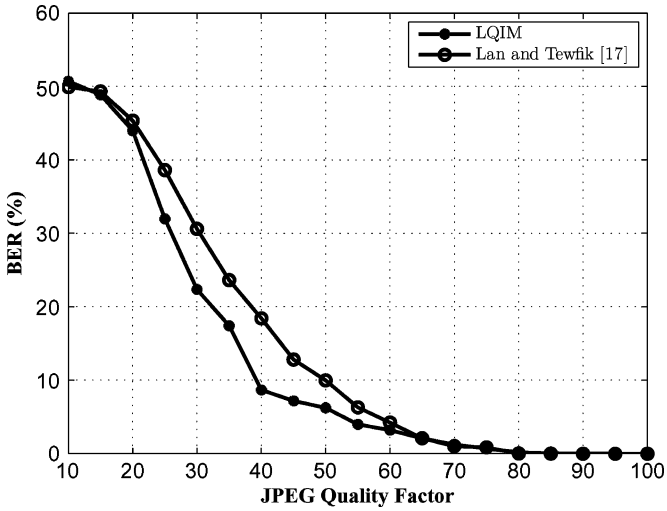

Fig. 15. BER(%) versus JPEG quality factor for JPEG compression attack. 12288 bits have been embedded within Lena image in both methods.

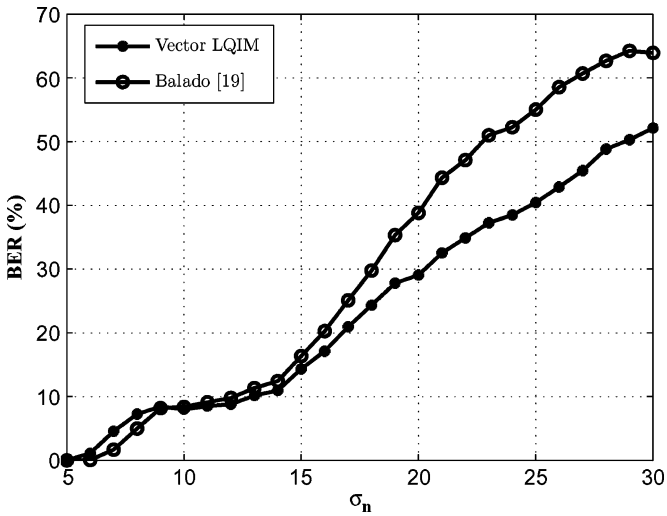

Fig. 16. BER (%) of watermark extraction under AWGN attack for various noise variances. 128 bits have been embedded within Lena image in both methods.

detection after AWGN attack is depicted in Fig. 16. Here, the results for some σ_n values are also presented in Table V. As seen again, the SHDM is better than vector LQIM in low attack power and in high noise variances, LQIM outperforms SHDM. It should be noted that since the shape parameter for the distribution of the selected coefficients is small, the analytical results do not match the empirical ones, and, thus, they are not included in this figure. Furthermore, the robustness of the proposed method in comparison with SHDM on ten well-known images was investigated and the average results are demonstrated in Fig. 17. As it can be seen, LQIM has better robustness in comparison with SHDM while simulation is performed on different images. Furthermore, comparison was made for data extraction BERs under some common attacks. Table VI demonstrates the results. As can be seen, LQIM has better performance than SHDM.

In order to investigate the effect of noise subtraction in vector case as mentioned in Section IV-B, we estimated the noise variance and subtracted it from s_r^2. The noise variance was estimated

TABLE V
RESULTS DEPICTED IN FIG. 16 FOR SOME σ_n VALUES

σ_n	BER (%)	
	vector LQIM	Balado [19]
5	0.0156	0
7	4.5625	1.6719
9	8.4219	8.2031
11	8.5	9.1094
13	10.1562	11.3281
15	14.3438	16.3594

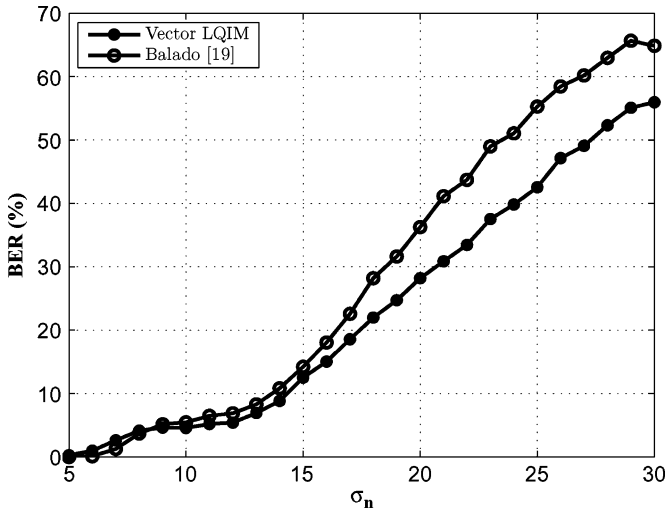

Fig. 17. BER (%) of watermark extraction under AWGN attack for various noise variances. The results are averaged over ten well-known images. 128 bits have been embedded within each image in both methods.

TABLE VI
BER(%) OF WATERMARK EXTRACTION FOR SOME COMMON ATTACKS. 4096 bits HAVE BEEN EMBEDDED IN LENA IMAGE IN BOTH METHODS. THE WINDOW SIZE FOR GAUSSIAN FILTER IS 3×3

Attacks		BER (%)	
		vector LQIM	Balado [19]
Median filtering	3×3	5.39	7.54
Gaussian filtering	$\sigma^2 = 0.5$	0	0.31
	$\sigma^2 = 0.7$	4.38	10.31
	$\sigma^2 = 0.9$	14.38	18.59

in the wavelet domain, using the robust median noise estimator proposed by Donoho and Johnstone in [20] as

$$\hat{\sigma}_n = \frac{\text{median}\,(|y_{i,j}|)}{0.6745}$$

where $y_{i,j}$ represents the diagonal detail coefficients of the first level. The performance of both schemes with noise subtraction under AWGN attack is demonstrated in Fig. 18. Comparing this figure with Fig. 16, the improvement in performance is obvious. Again, the analytical predictions are not included in this figure for the reason mentioned in the previous paragraph.

Finally, we tested both methods under the JPEG compression attack and the results are presented in Fig. 19. As is clear, vector LQIM results in better performance in comparison with SHDM which uses uniform quantization.

Due to vulnerability of quantization to amplitude scaling, the proposed method would also suffer from gain attack. How-

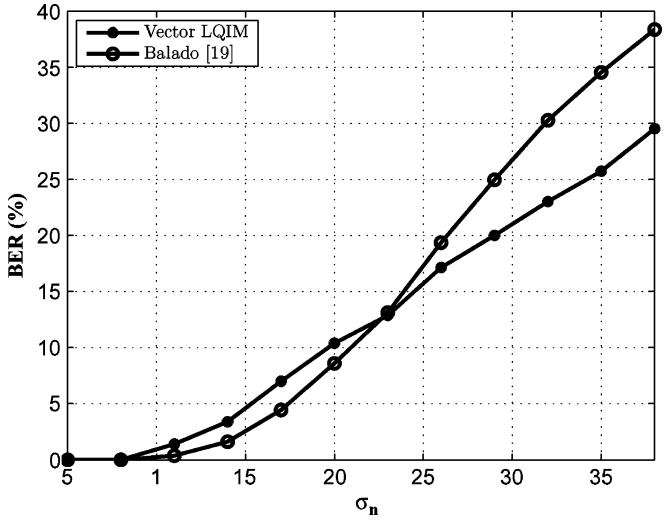

Fig. 18. BER (%) of watermark extraction with noise subtraction scheme under AWGN attack for various noise variances. 128 bits have been embedded within Lena image in both methods.

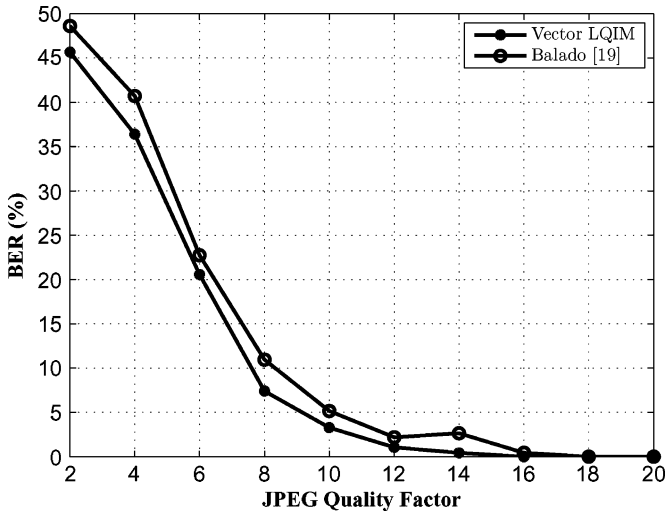

Fig. 19. BER(%) versus JPEG quality factor for JPEG compression attack. 128 bits have been embedded within Lena image in both methods.

ever, an interesting approach named Rational Dither Modulation (RDM) has been proposed in [16] which lets us alleviate this problem. RDM uses a division function to overcome the gain attack. A similar approach with slight modification can be used here. However, obtaining the appropriate value for μ in this case and investigation of its performance is beyond the scope of this paper and is a good direction for future research.

VII. Conclusion

In this paper, a novel quantizer arrangement for quantization-based data hiding, called LQIM, was proposed. Inspired by μ-Law concept, the host signal was transformed into logarithmic domain using a compression function. Then, data was embedded into the transformed signal using uniform quantization and the quantized data was transformed into the original domain using inverse function. Due to the use of logarithmic function, smaller step sizes are devoted to smaller amplitudes and larger step sizes are associated with larger amplitudes. Therefore, in comparison with UQIM, this method poses perceptual advantages that lead to stronger watermark insertion. Furthermore, this method has not the drawbacks of a previous logarithmic quantization-based method proposed in [5]. The scalar case was also extended to vector LQIM by quantizing the magnitude of the host signal vector using the proposed method. The optimum parameter was also found regarding the host signal distribution, by use of which minimum quantization distortion is introduced to the host signal. Furthermore, the probability of error was obtained for both scalar and vector LQIM and the validity of theoretical results was experimentally verified. Moreover, data hiding using secret key was proposed. Simulations show better robustness of the proposed method in comparison with previous quantization-based algorithms, in similar perceptual qualities of watermarked images.

References

[1] B. Chen and G. Wornell, "Quantization index modulation: A class of provably good methods for digital watermarking and information embedding," *IEEE Trans. Inf. Theory*, vol. 47, no. 4, pp. 1423–1443, May 2001.

[2] P. Moulin and R. Koetter, "Data-hiding codes," *Proc. IEEE*, vol. 93, no. 12, pp. 2083–2127, Dec. 2005.

[3] J. Chou, K. Ramchandran, and A. Ortega, "Next generation techniques for robust and imperceptible audio data hiding," in *Proc. IEEE Int. Conf. Acoustics, Speech, Signal Processing (ICASSP)*, May 2001, vol. 3, pp. 1349–1352.

[4] J. Eggers and B. Girod, *Informed Watermarking*. Norwell, MA: Kluwer, 2002.

[5] P. Comesana and F. Perez-Gonzalez, "On a watermarking scheme in the logarithmic domain and its perceptual advantages," presented at the IEEE Int. Conf. Image Processing, San Antonio, TX, Sep. 2007.

[6] I. J. Cox, J. Kilian, T. Leighton, and T. Shamoon, "Secure spread spectrum watermarking for multimedia," *IEEE Trans. Image Process.*, vol. 6, no. 12, pp. 1673–1687, Dec. 1997.

[7] M. Barni, F. Bartolini, A. De Rosa, and A. Piva, "A new decoder for the optimum recovery of non-additive watermarks," *IEEE Trans. Image Process.*, vol. 10, no. 5, pp. 755–766, May 2001.

[8] M. Barni, C. I. Podilchuk, F. Bartolini, and E. J. Delp, "Watermark embedding: Hiding a signal within a cover image," *IEEE Commun. Mag.*, vol. 39, no. 8, pp. 102–108, Aug. 2001.

[9] F. A. P. Petitcolas and S. Katzenbeisser, *Information Hiding: Techniques for Steganography and Digital Watermarking*, 1st ed. Boston, MA: Artech House, 2000.

[10] I. J. Cox and J.-P. M. G. Linnartz, "Some general methods for tampering with watermarks," *IEEE J. Sel. Areas Commun.*, vol. 16, no. 4, pp. 587–593, May 1998.

[11] J. R. Deller, Jr., J. G. Proakis, and J. H. L. Hansen, *Discrete Time Processing of Speech Signals*. New York: Macmillan, 1993.

[12] Q. Cheng and T. S. Huang, "Robust optimum detection of transform domain multiplicative watermarks," *IEEE Trans. Signal Process.*, vol. 51, no. 4, pp. 906–924, Apr. 2003.

[13] J. Zhong and S. Huang, "Double sided watermark embedding and detection," *IEEE Trans. Inf. Forens. Sec.*, vol. 2, no. 3, pp. 297–310, Sep. 2007.

[14] A. Nikolaidis and I. Pitas, "Asymptotically optimal detection for additive watermarking in the DCT and DWT domains," *IEEE Trans. Image Process.*, vol. 12, no. 5, pp. 563–571, May 2003.

[15] J. A. Dominguez-Molina, G. Gonzalez-Farias, and R. M. Rodriguez-Dagnino, A Practical Procedure to Estimate the Shape Parameter in the Generalized Gaussian Distribution, CIMAT Tech. Rep. I-01-18_eng.pdf [Online]. Available: http://www.cimat.mx/reportes/enlinea/I-01-18_eng.pdf

[16] F. Perez-Gonzalez, C. Mosquera, M. Barni, and A. Abrardo, "Rational Dither Modulation: A high-rate data-hiding method robust to gain attacks," *IEEE Trans. Signal Process.*, vol. 53, no. 10, pp. 3960–3975, Oct. 2005, 3rd supplement on secure media.

[17] T. H. Lan and A. H. Tewfik, "A novel high-capacity data-embedding system," *IEEE Trans. Image Process.*, vol. 15, no. 8, pp. 2431–2440, Aug. 2006.

[18] A. B. Watson, "DCT quantization matrices optimized for indivudual images," presented at the SPIE Human Vision, Visual Processing, and Digital Display IV, 1993, vol. 1913.
[19] F. Balado, "New geometric analysis of spread-spectrum data hiding with repetition coding, with implications for side-informed schemes," in *Proc. IWDW*, Siena, Italy, Sep. 2005, pp. 336–350.
[20] D. L. Donoho and I. M. Johnstone, "Ideal spatial adaptation via wavelet shrinkage," *Biometrica*, vol. 81, pp. 425–455, 1994.

Nima Khademi Kalantari (S'09) was born in Tehran, Iran, in 1984. He received the B.Sc. degree in electrical engineering in 2007 from the Amirkabir University of Technology, Tehran, Iran, where he is currently pursuing the M.Sc. degree.

His research interests include multimedia security, image and speech processing, and statistical signal processing.

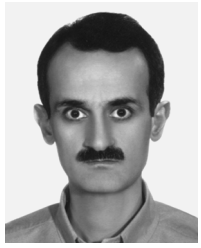

Seyed Mohammad Ahadi (M'87–SM'03) received the B.Sc. and M.Sc. degrees in electronics from the Electrical Engineering Department, Amirkabir University of Technology, Tehran, Iran, in 1984 and 1987, respectively, and the Ph.D. degree in engineering from the University of Cambridge, Cambridge, U.K., in 1996, working in the field of speech recognition.

He was appointed faculty member in the Electrical Engineering Department, Amirkabir University of Technology, in 1988, where he began his teaching profession as well as involvement in research projects. Since receiving the Ph.D. degree, he has been with the same department, where he is currently the Head of the Electronics Group, teaching several courses and conducting research in electronics and communications.